Using nodal seismic sensors to estimate seismic moment tensors

Part B: Seismic moment tensors

Cole Richards

Last compiled : November 26, 2019

This is Part B of the collection; see also Part A, which focuses on amplitude response of nodal seismic stations.

Overview: This document demonstrates the use of nodal seismic sensors in body wave moment tensors inversions. The nodal sensors used in this study are Geo Space GS-30CT/FairfieldNodal ZLAND 3C sensors.

Data proccesing

We use the open-source software repository `pysep` to fetch and process seismic waveforms from the IRIS DMC. `pysep` employs ObsPy (*Beyreuther et al.*, 2010; *Krischer et al.*, 2015). All waveforms are resampled to 50 Hz, are scaled by 100, and have the instrument response removed with obspy's default water level of 60.

Event selection

For the inversions we select an aftershock
2019-02-18 17:02:46.710 lon -149.96 lat 61.47 dep 37.60 km Ml 4.40
of the 2018-11-30 M_{w} 7.1 Anchorage earthquake. We also use a local event that occurred nearly directly beneath the nodal transect:
2019-02-25 18:22:30.906 lon -149.62 lat 62.80 dep 73.70 km Ml 3.10.

Estimation of seismic moment tensors

The output figures include: 1) a large beachball (e.g., Figure M4), 2) a comparison of observed and modeled waveforms (e.g.,, Figure M3), and 3) a depth grid search (e.g., Figure M1). Details about the content in these figures can be found in *Richards* (2019). In many cases, the plotted waveforms are extremely small, but they should be visible when zoomed way into the pdf file.

For the local event, Figure M1 shows a grid search over depth and magnitude for three different station subsets: permanent stations only, nodal stations only, and both permanent and nodal stations together. The combination of both the permanent and nodal stations has a best-fitting solution that is close to the Alaska Earthquake Center (AEC) catalog depth and the mechanism is mostly stable as depth changes. Including the nodes adds an impressive distribution of station coverage on the focal sphere (compare Figure M4 to Figure M6). While using only nodal stations does find a best-fitting solution with a similar mechanism and depth to the combined station solution, the mechanism changes drastically at deeper depths. The permanent station only best-fitting solution is a similar mechanism but the depth of 58.1 ± 4.8 km is too shallow. There is a local mimimum at 70 km that would make more sense as the best solution. Figure M5 and Figure M6 show the moment tensor solution when using permanent stations only. Figure M3

and Figure M4 show the moment tensor solution when using the exact same permanent stations while also including nodal stations.

Finally, as a warning, good waveform fits do not always imply an accurate solution. Figure M14 and Figure M15 show the best-fitting solution for nodes only with 1.5 second allowable time shifts from Figure M9. The waveforms fit well, but as we have shown, this mechanism is probably not correct. For the aftershock, Figure M18 and Figure M19 show the moment tensor solution when using permanent stations only. Figure M16 and Figure M17 show the moment tensor solution when using both the permanent stations and nodal stations. The addition of the nodes changes the mechanism slightly and improve the variance reduction. Using the nodal stations for surface wave inversions at longer periods ought to be possible for larger events but surface waves were not included in these inversion due to low SNR. However, when using longer periods it is important to use a high water level when removing the instrument response of the nodes. In Part A of this collection, we show that at the default water level of 60, that the amplitudes of the nodal stations is too low when compared to neighboring broad band sensors at 10–20 s.

Time shifts and cycle skipping

For the inversions we must choose a maximum allowable time shift between data and synthetic waveforms. For all three station subsets we examined 1.5 and 2.5 second allowable time shifts. In order to have proper waveform fits at some distant stations a 2.5 second time shift is required. For example, permanent station PAX at 212 km has good fitting waveforms in Figure M3 which has 2.5 second allowable time shifts. However, in Figure M10, station PAX is cycle skipped due to the shorter 1.5 second allowable time shifts. On the contrary, nodal station 1253 at 153 km is cycle skipped in the 2.5 second but not in the 1.5 second solution. Overall, we favor 2.5 second allowable time shifts as their best-fitting solutions are closest to the AEC catalog depth compared to much deeper solutions produced by a 1.5 second allowable time shift. Figure M1 shows the 2.5 second time shift solutions and their respective waveform fits and beach balls are shown in Figure M5, Figure M6, Figure M3, and Figure M4. Figure M9 shows the 1.5 second time shift solutions and their respective waveform fits and beach balls are shown in Figure M12, Figure M13, Figure M10, and Figure M11.

References

Beyreuther, M., R. Barsch, L. Krischer, T. Megies, Y. Behr, and J. Wassermann (2010), ObsPy: A Python toolbox for seismology, *Seismol. Res. Lett.*, *81*(3), 530–533, doi:10.1785/gssrl.81.3.530.

Krischer, L., T. Mengies, R. Barsch, M. Beyreuther, T. Lecocq, C. Caudron, and J. Wassermann (2015), ObsPy: a bridge for seismology into the scientific Python ecosystem, *Computational Science & Discovery*, *8*(1), 014003, doi:10.1088/1749-4699/8/1/014003.

Richards, C. (2019), Moment tensors for the mainshock and aftershocks of the 2018-11-30 M_w 7.1 Anchorage earthquake, ScholarWorks@UA at `http://hdl.handle.net/11122/10173` (last accessed 2019-05-16): descriptor files, text file of catalog, and figures of waveform fits.

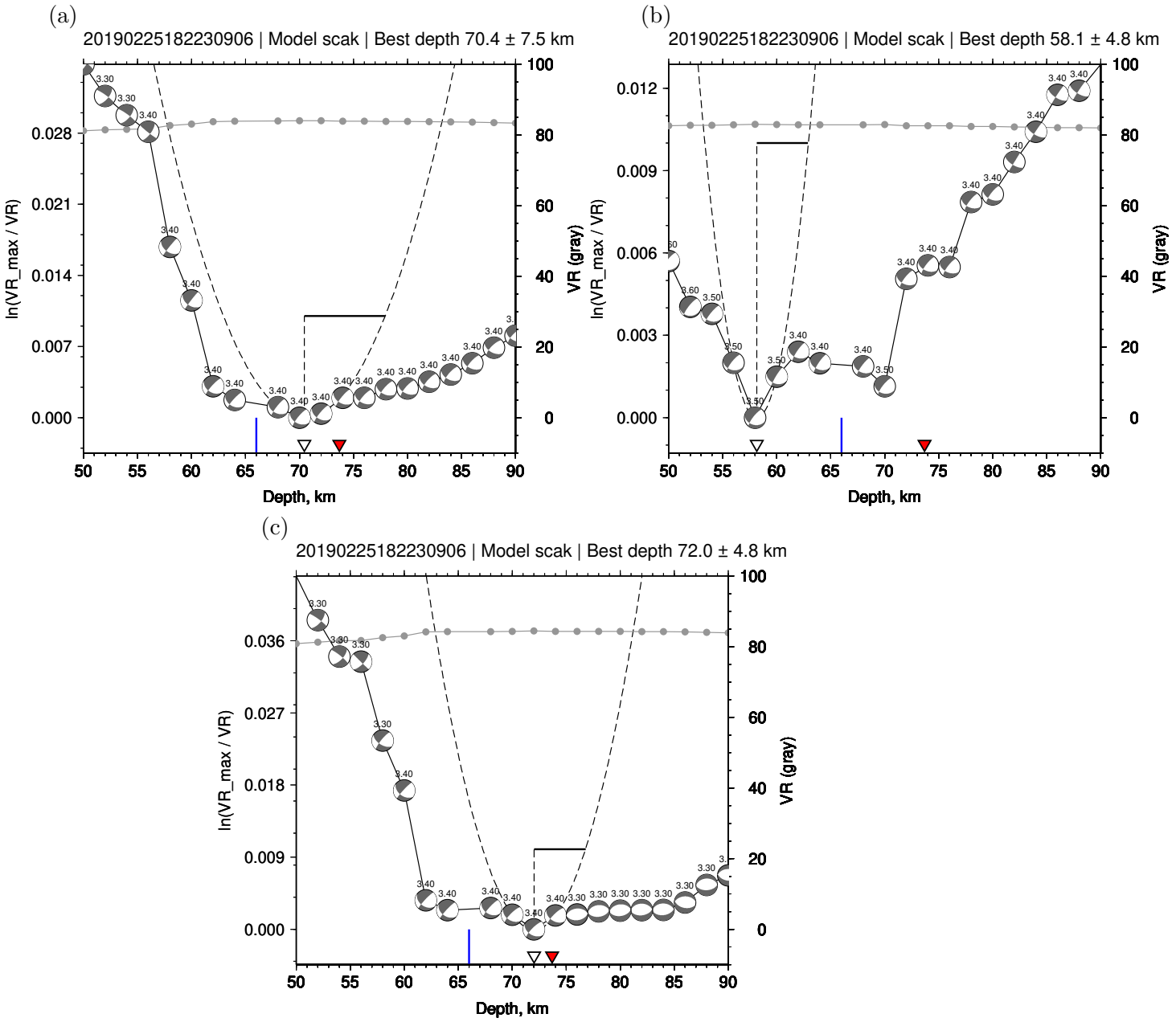

Figure M1: Grid search over depth and magnitude for moment tensors of the Cantwell local event. At each depth, the best-fitting moment tensor (including magnitude) is shown. The magnitude search increment is $\Delta M_{\mathrm{w}} = 0.1$; the depth search increment is 2 km. The allowable time shift between data and synthetic waves forms is 2.5 seconds. The red triangle denotes the AEC catalog depth of 74 km, which is obtained from P and S arrival times. The blue lines on the x-axis denote the layer boundaries in the 1D velocity model. (a) Permanent stations only. Best-fitting depth is 58.1 ± 4.8 km. (b) Nodal stations only. Best-fitting depth is 72.0 ± 4.8 km. (c) Permanent and nodal stations. Best-fitting depth is 70.4 ± 7.5 km.

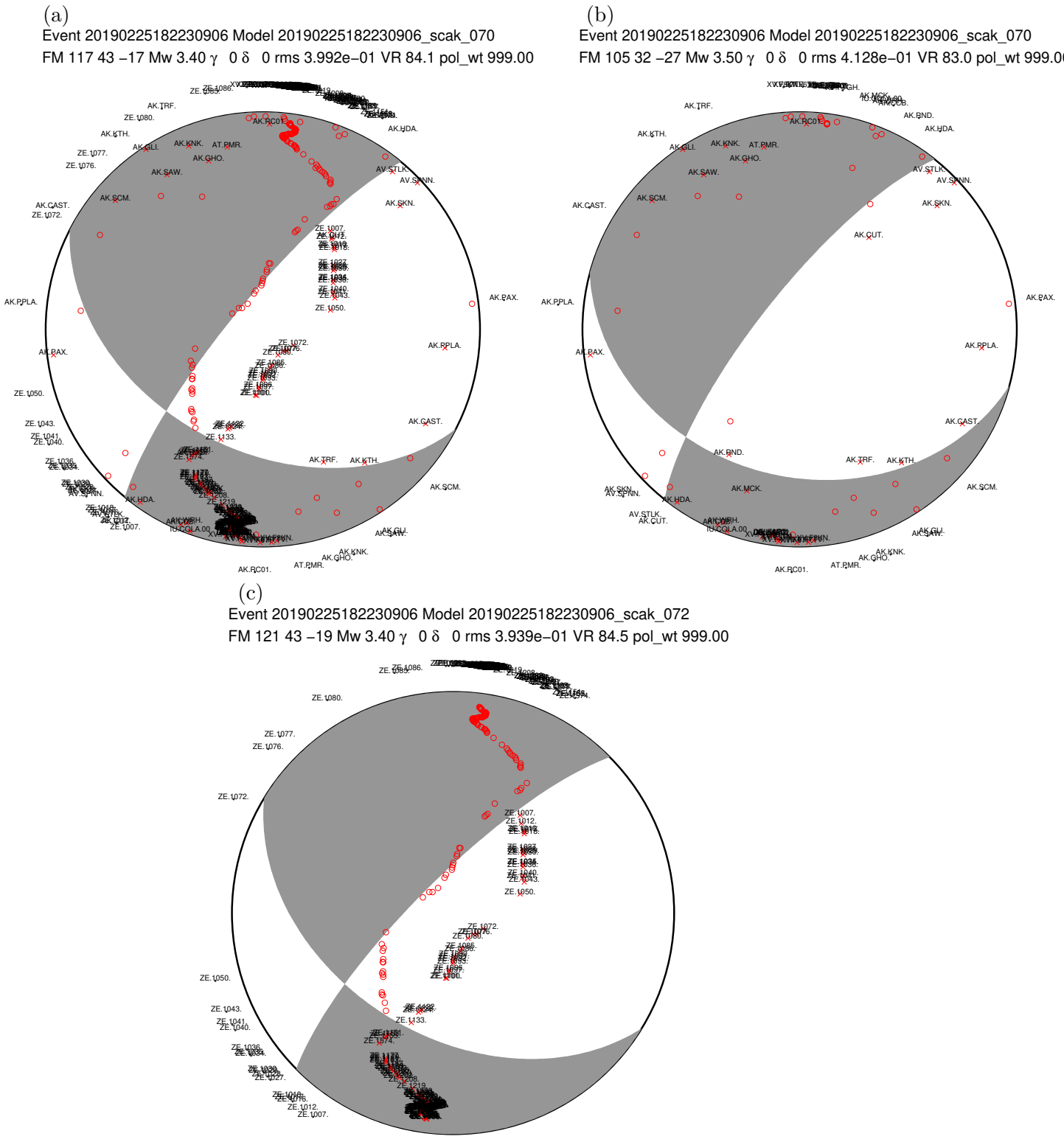

Figure M2: Best-fitting moment tensors for the local Cantwell event with 2.5 second allowable time shifts. (a) Permanent and nodal stations. Best-fitting depth is 82.9 ± 7.3 km. (b) Permanent stations only. Best-fitting depth is 82.6 ± 4.5 km. (c) Nodal stations only. Best-fitting depth is 83.5 ± 7.5 km. X symbols show the lower-hemisphere piercing points of the ray paths to each station used in the moment tensor search. The text labels on the outside denote the station directions (azimuths) relative to the source. The magnitude and depth are obtained using an increment of $\Delta M_{\mathrm{w}} = 0.1$ and $\Delta\ km = 2$. Grid searches are shown in Figure M1

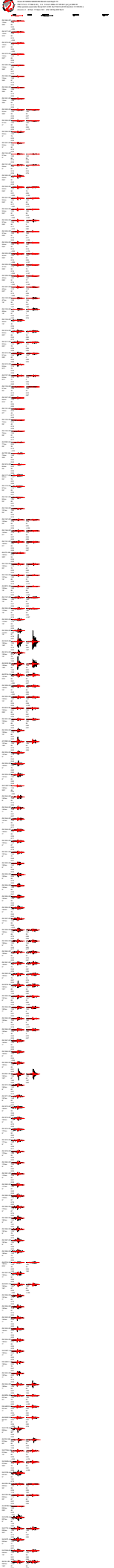

Figure M3: Best-fitting moment tensor and waveform fits for event 20190225182230906. Red = time-shifted synthetics, black = data. For each station, the five time windows are for P wave vertical (PV), P wave radial (PR), Rayleigh waves (Surf V, Surf R), and Love waves (Surf T). Numbers beneath each waveform pair are the time shift, the cross correlation maximum, the percentage of the misfit function, and the log amplitude ratio. The stations are sorted by azimuth from 0–360 degrees (relative to the source). Note: only body waves were used in the inversion. The allowable time shift between data and synthetic waves forms is 2.5 seconds. This solution includes both permanent and nodal stations.

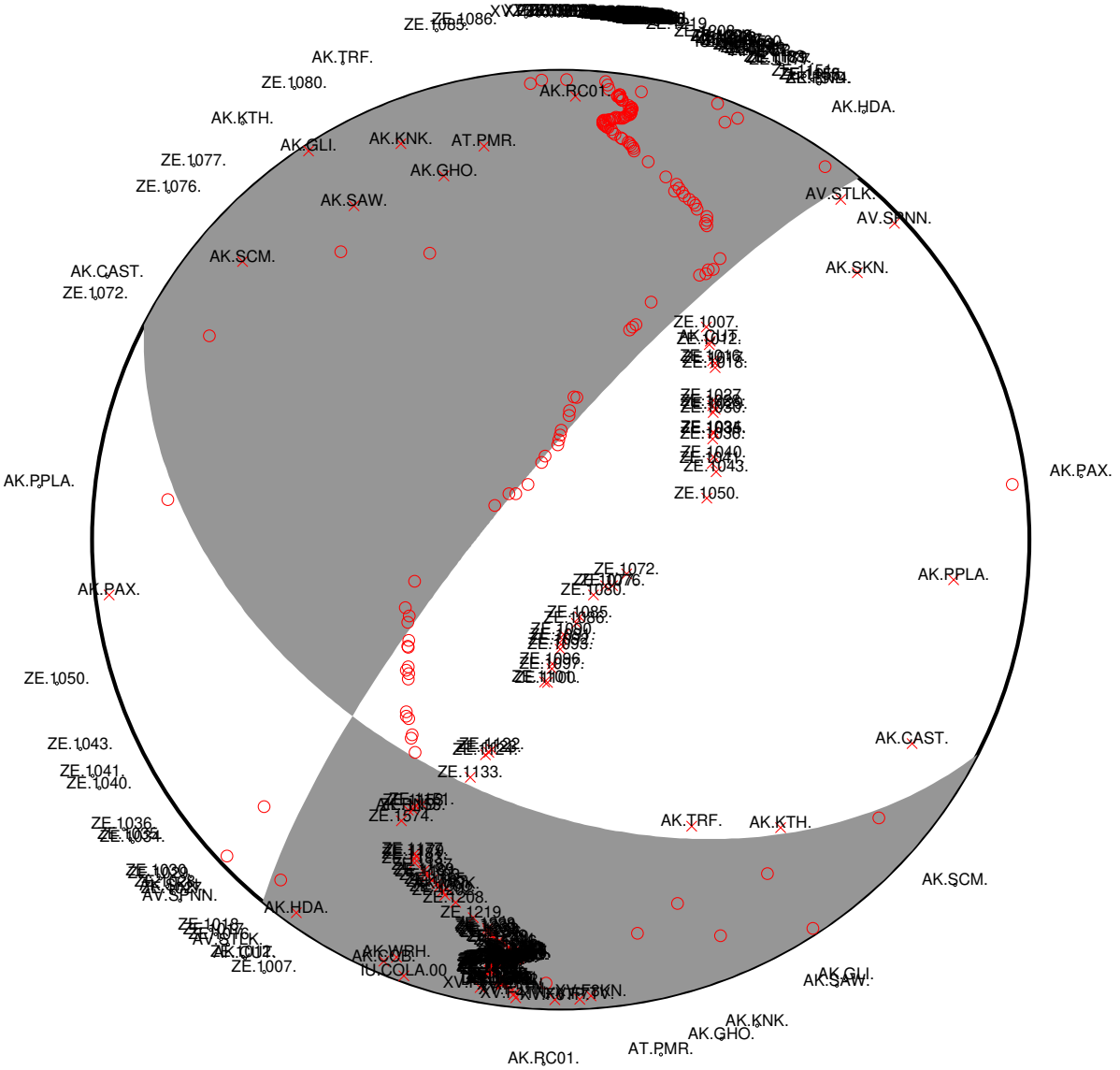

Figure M4: Best-fitting moment tensor for a M_w 3.40 located beneath the nodal transect. X symbols show the lower-hemisphere piercing points of the ray paths to each station used in the moment tensor search. The text labels on the outside denote the station directions (azimuths) relative to the source. The magnitude and depth are obtained using an increment of $\Delta M_w = 0.1$ and $\Delta\ km = 2$. Figure M3 displays the waveform fits for this event. This solution includes both permanent and nodal stations.

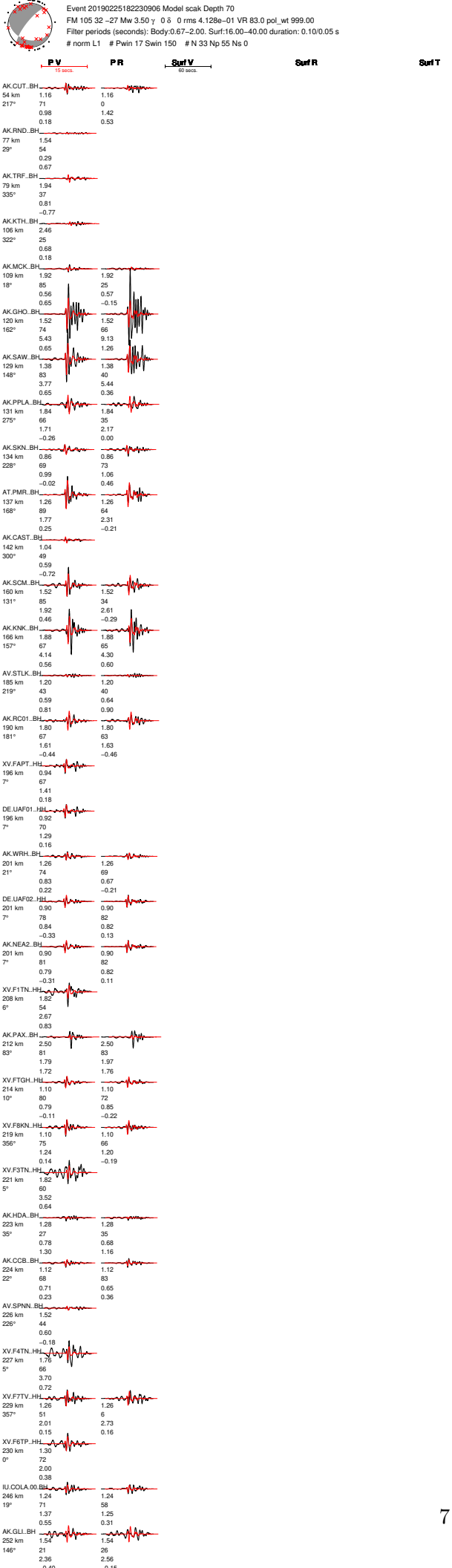

Figure M5: Same as Figure M3 except this solution includes only permanent stations.

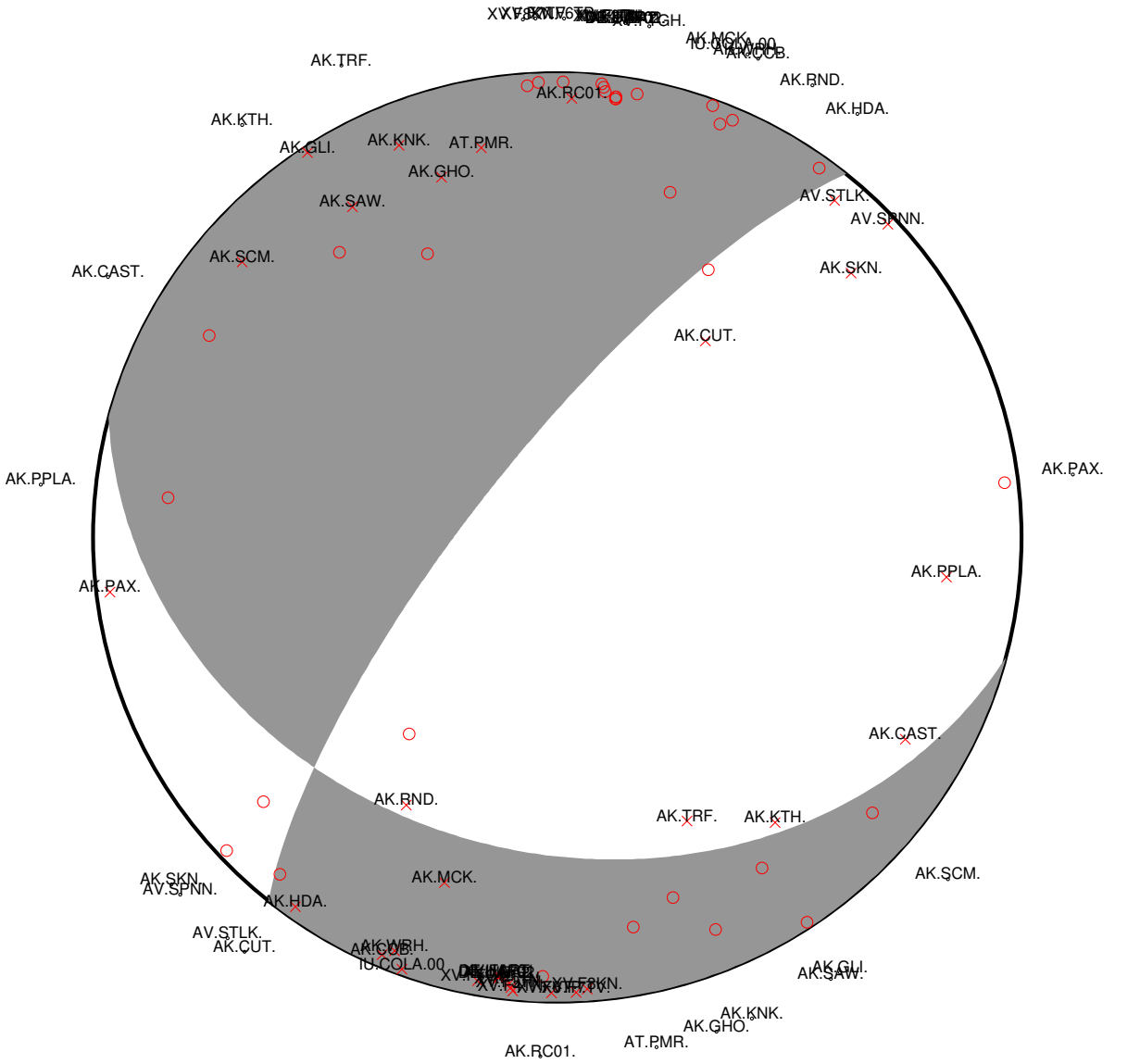

Figure M6: Same as Figure M4 except this solution includes only permanent stations. Figure M5 displays the waveform fits for this event.

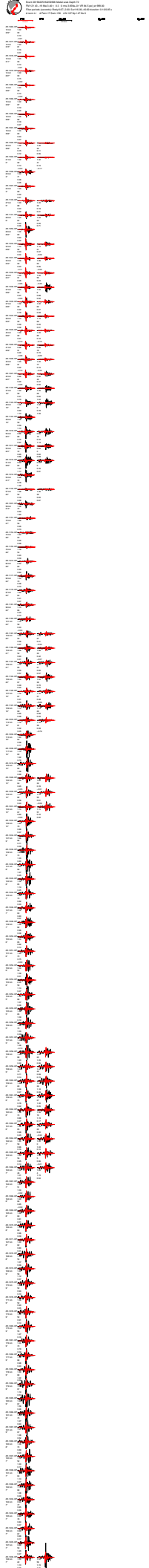

Figure M7: Same as Figure M3 except this solution includes only nodal stations.

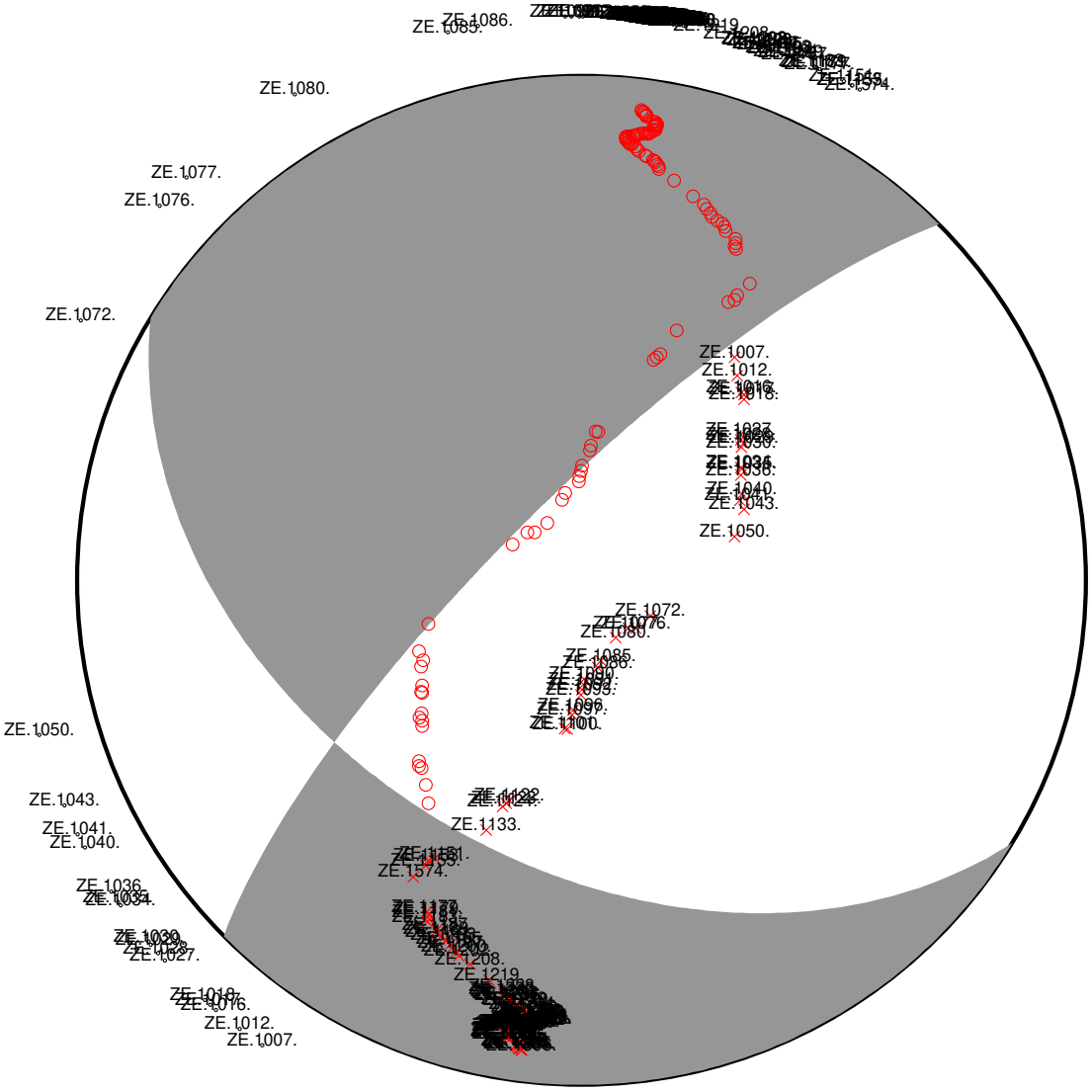

Figure M8: Same as Figure M4 except this solution includes only nodal stations. Figure M7 displays the waveform fits for this event.

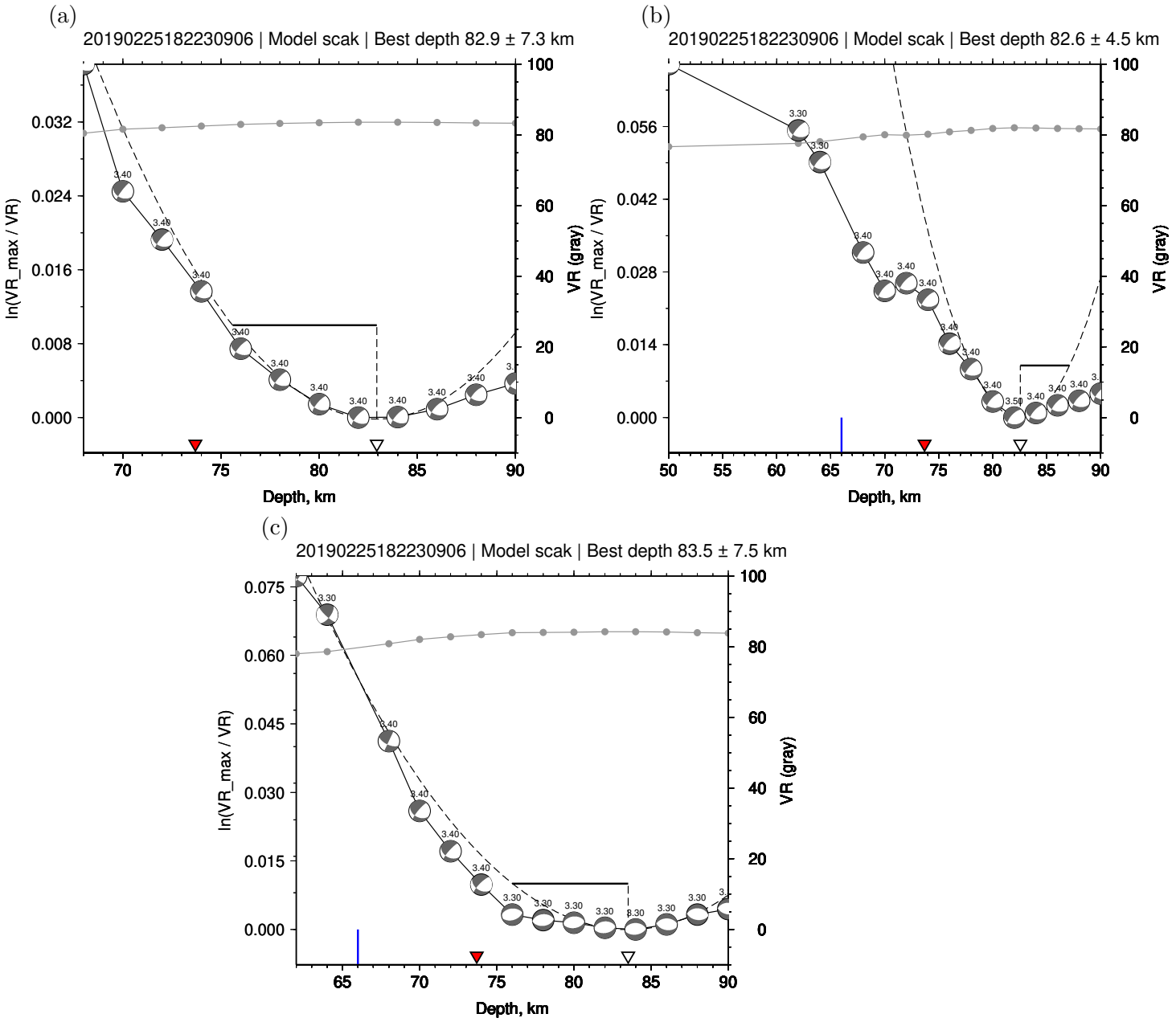

Figure M9: Same as Figure M1 except with 1.5 second allowable time shifts. (a) Permanent and nodal stations. Best-fitting depth is 82.9 ± 7.3 km. (b) Permanent stations only. Best-fitting depth is 82.6 ± 4.5 km. (c) Nodal stations only. Best-fitting depth is 83.5 ± 7.5 km.
Notice that the the shorter allowable time shift pushes the best-fitting solution further from the AEC catalog solution and some stations are now cycle skipped (see PAX at 212 km in Figure M10) suggesting that the 2.5 second time shift solution (Figure M1, Figure M3, Figure M4) is the better choice.

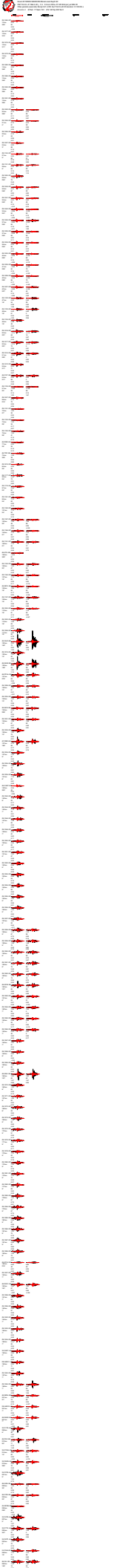

Figure M10: Same as Figure M3 except with 1.5 second allowable time shifts.

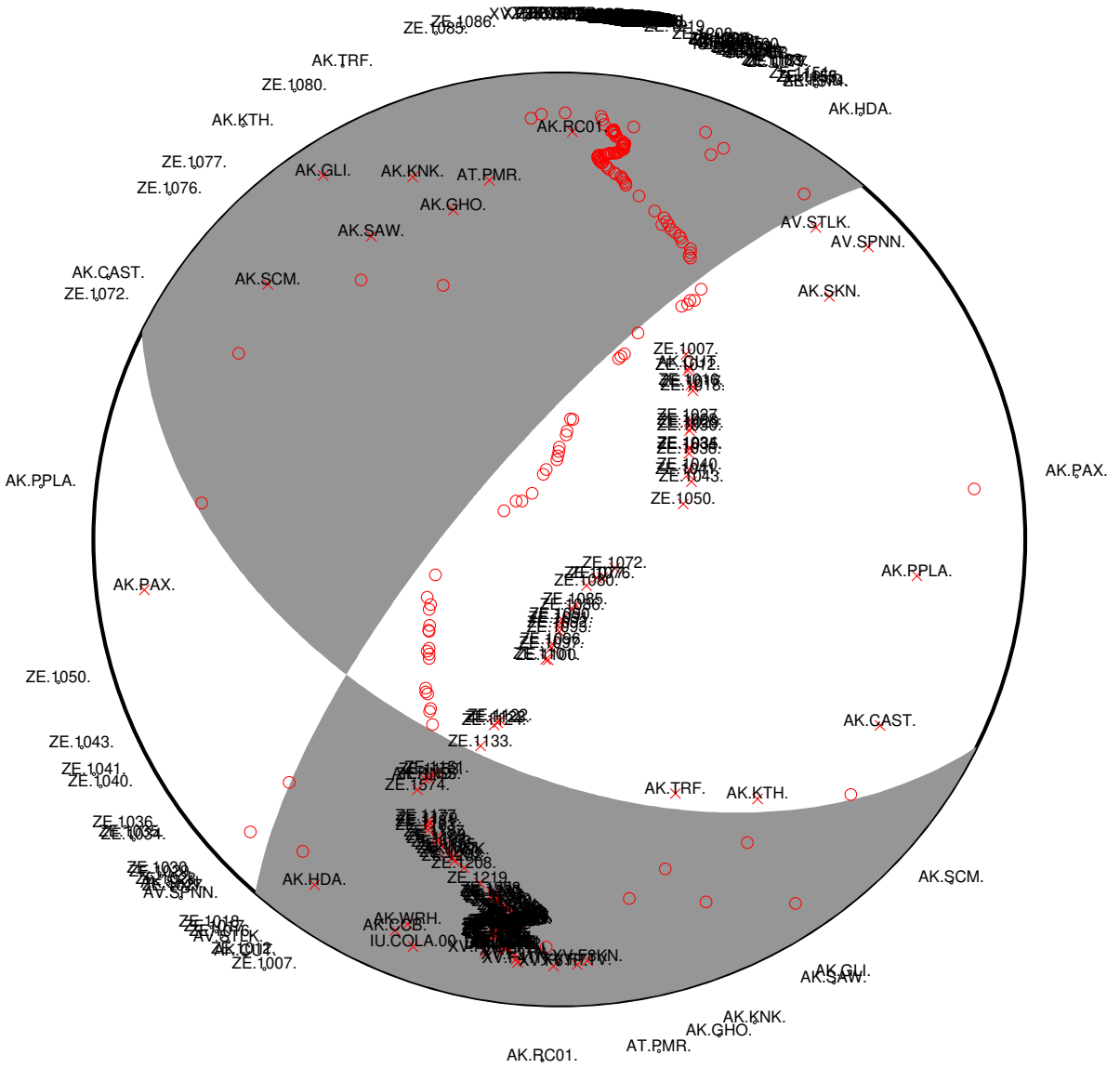

Figure M11: Same as Figure M4 except with 1.5 second allowable time shifts. Figure M10 displays the waveform fits for this event.

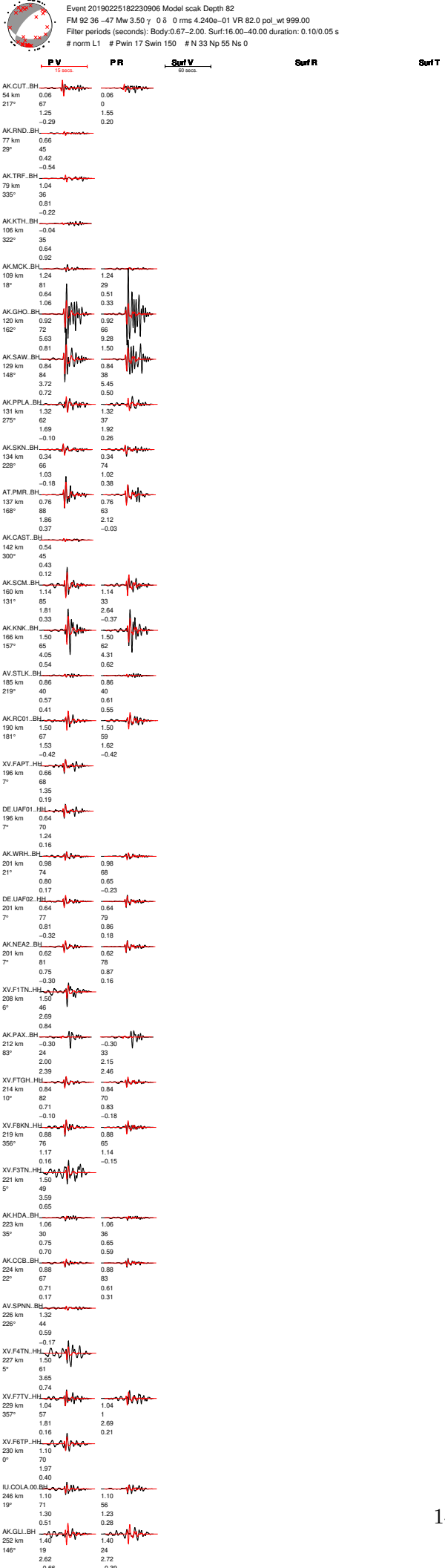

Figure M12: Same as Figure M3 except this solution includes only permanent stations and has 1.5 second allowable time shifts.

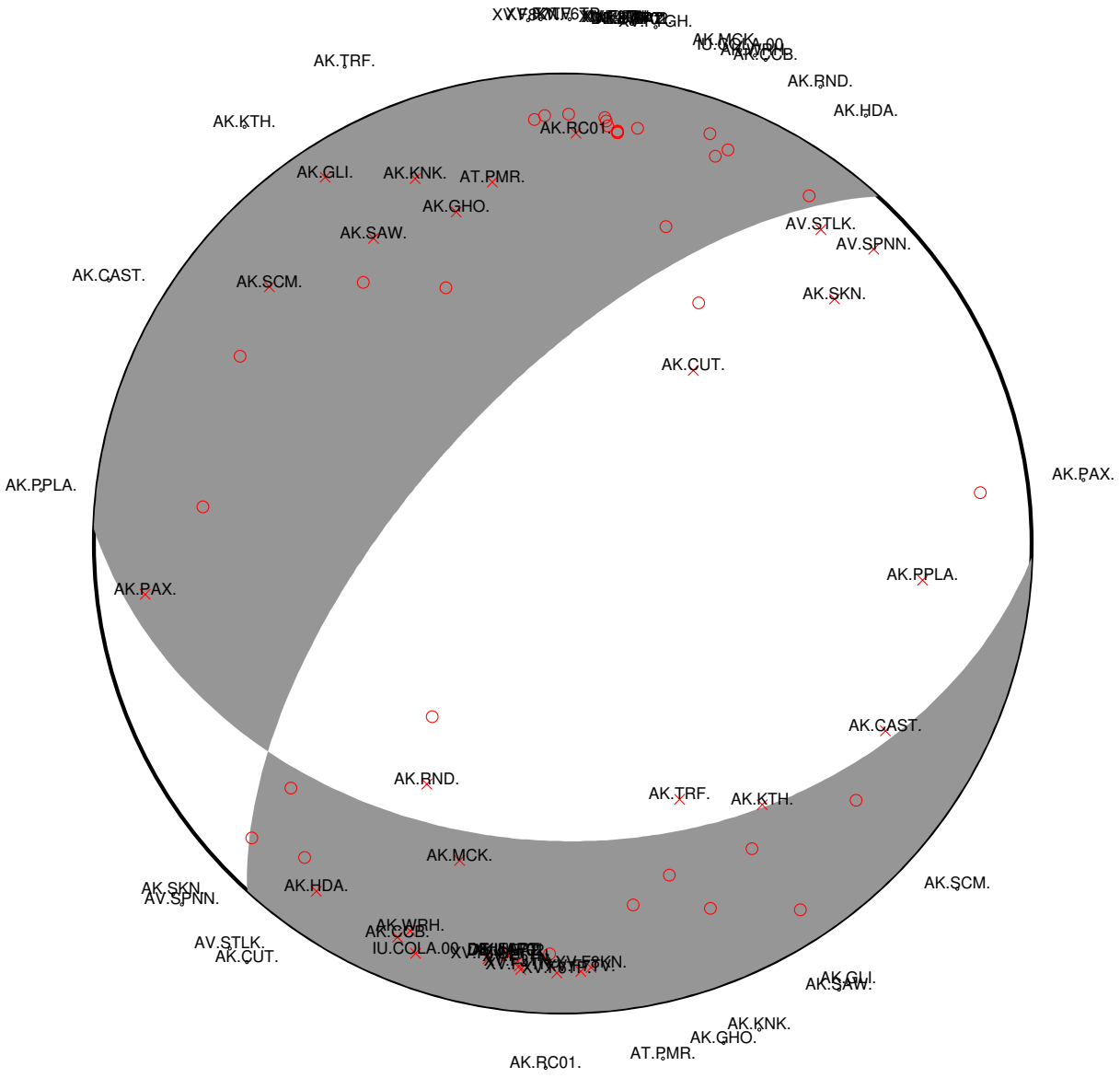

Figure M13: Same as Figure M4 except this solution includes only permanent stations and has 1.5 second allowable time shifts. Figure M12 displays the waveform fits for this event.

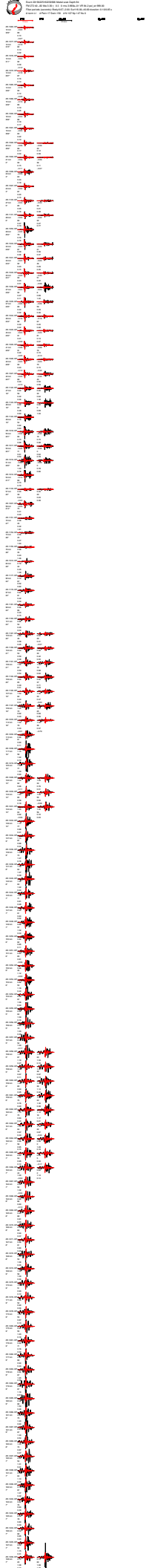

Figure M14: Same as Figure M3 except this solution includes only nodal stations and has 1.5 second allowable time shifts.

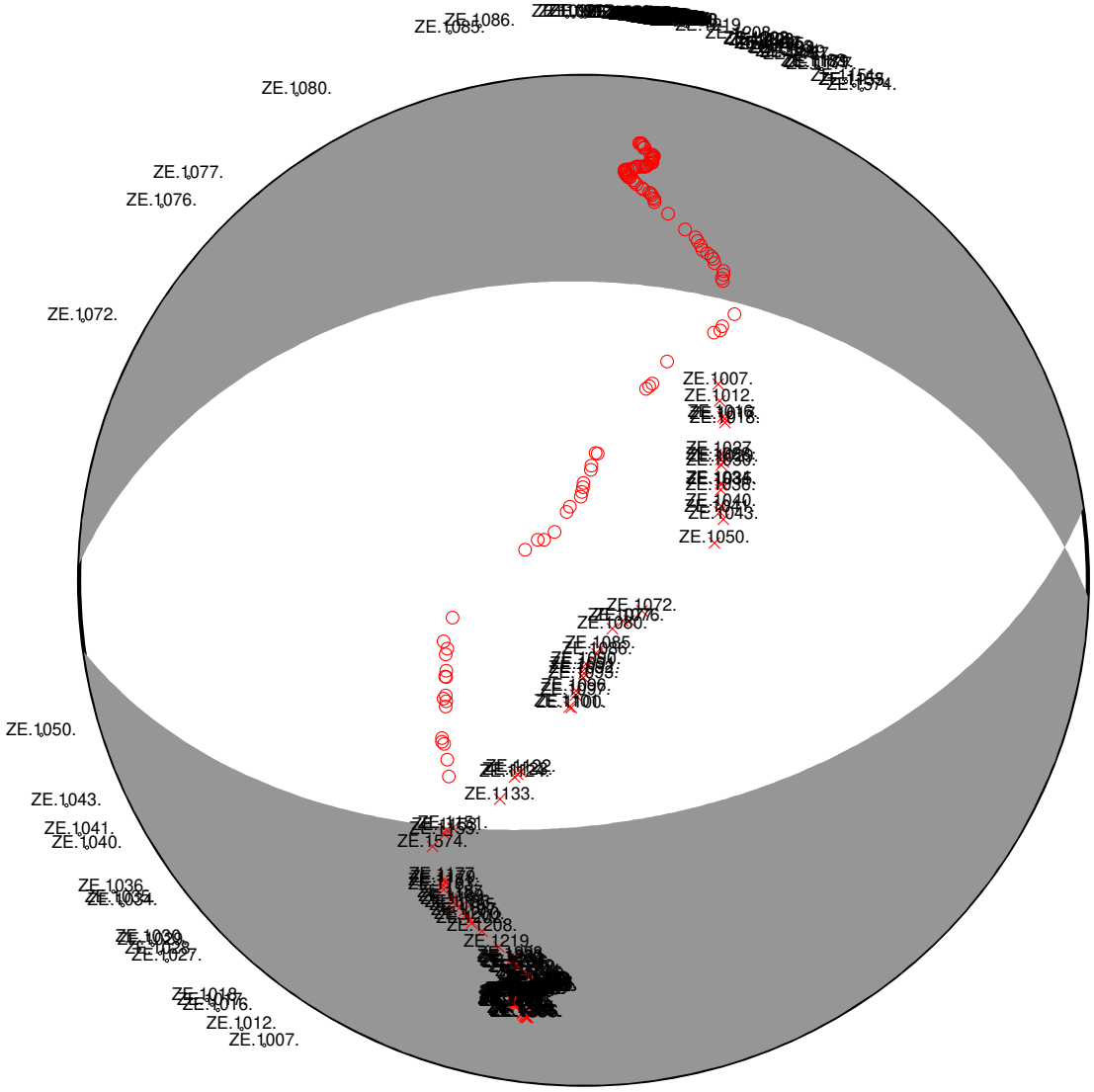

Figure M15: Same as Figure M4 except this solution includes only nodal stations and has 1.5 second allowable time shifts. Figure M14 displays the waveform fits for this event.

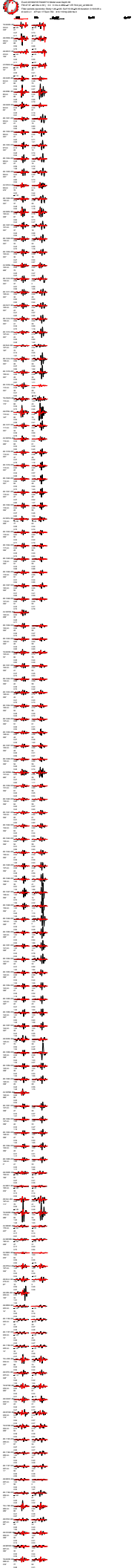

Figure M16: Same as Figure M3 except this is a solution for the 2018-11-30 M_{w} 7.1 Anchorage earthquakeaftershock and has 1 second allowable time shifts.

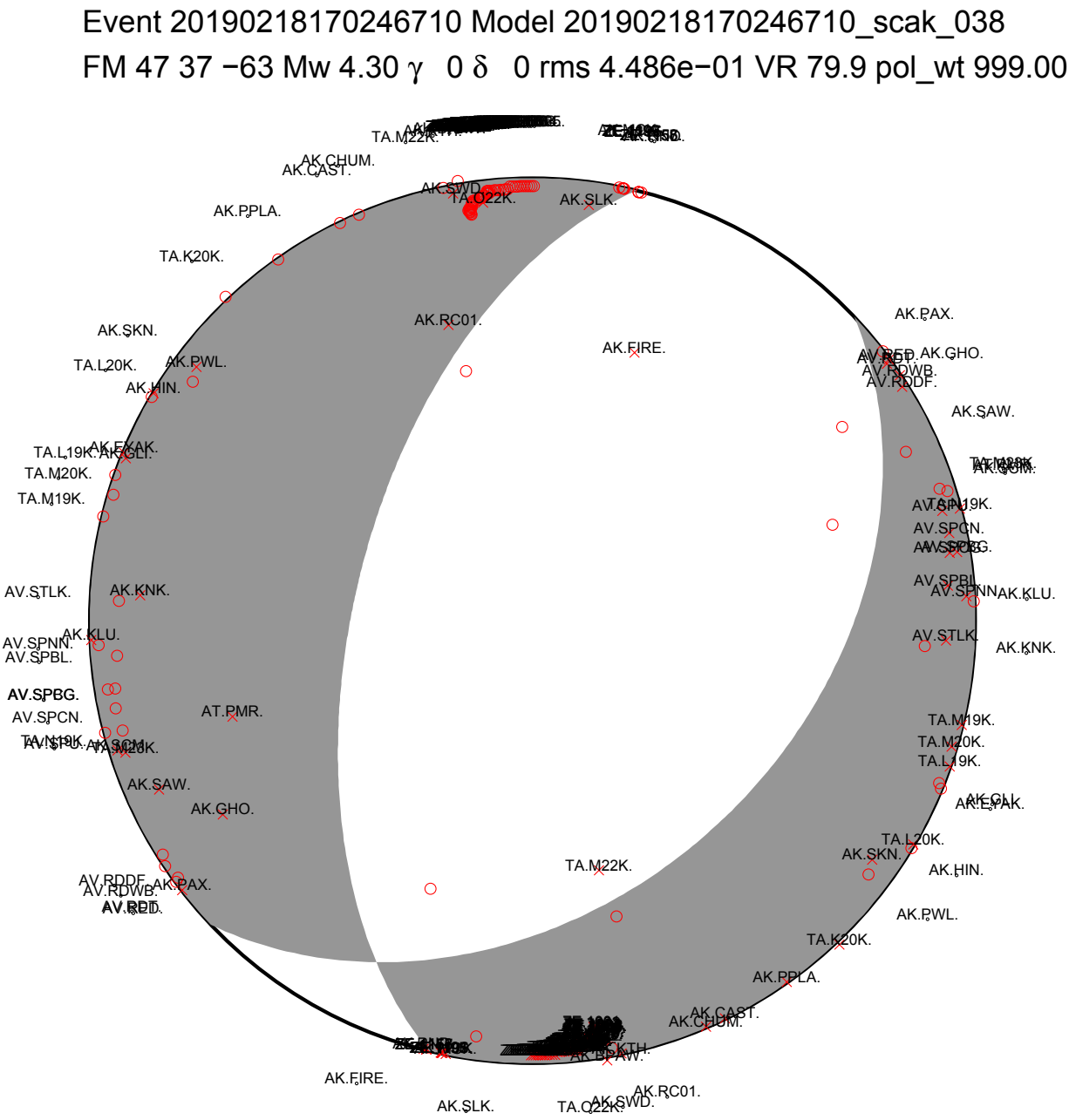

Figure M17: Same as Figure M4 except this is a solution for the 2018-11-30 M_w 7.1 Anchorage earthquakeaftershock and has 1 second allowable time shifts. Figure M16 displays the waveform fits for this event.

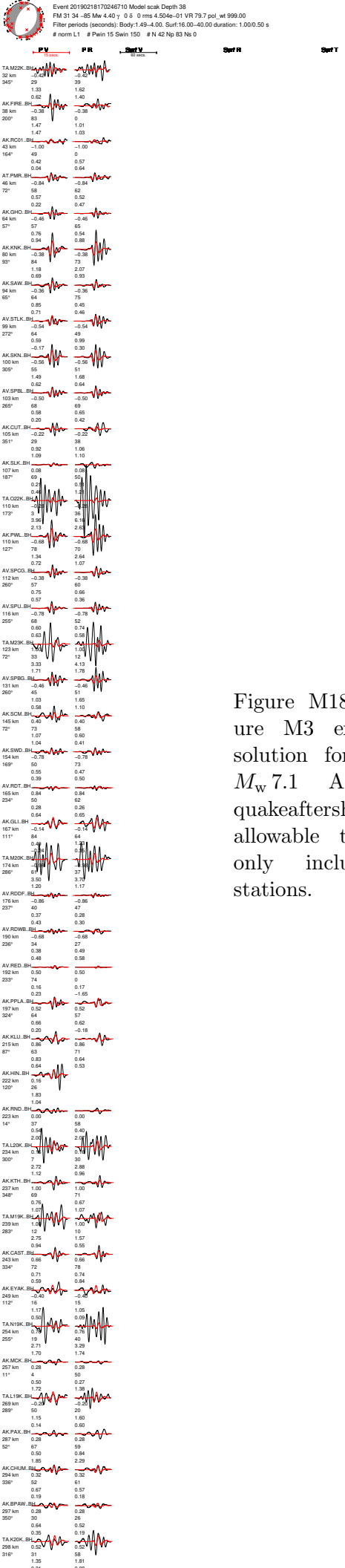

Figure M18: Same as Figure M3 except this is a solution for the 2018-11-30 M_{w} 7.1 Anchorage earthquakeaftershock, has 1 second allowable time shifts, and only includes permanent stations.

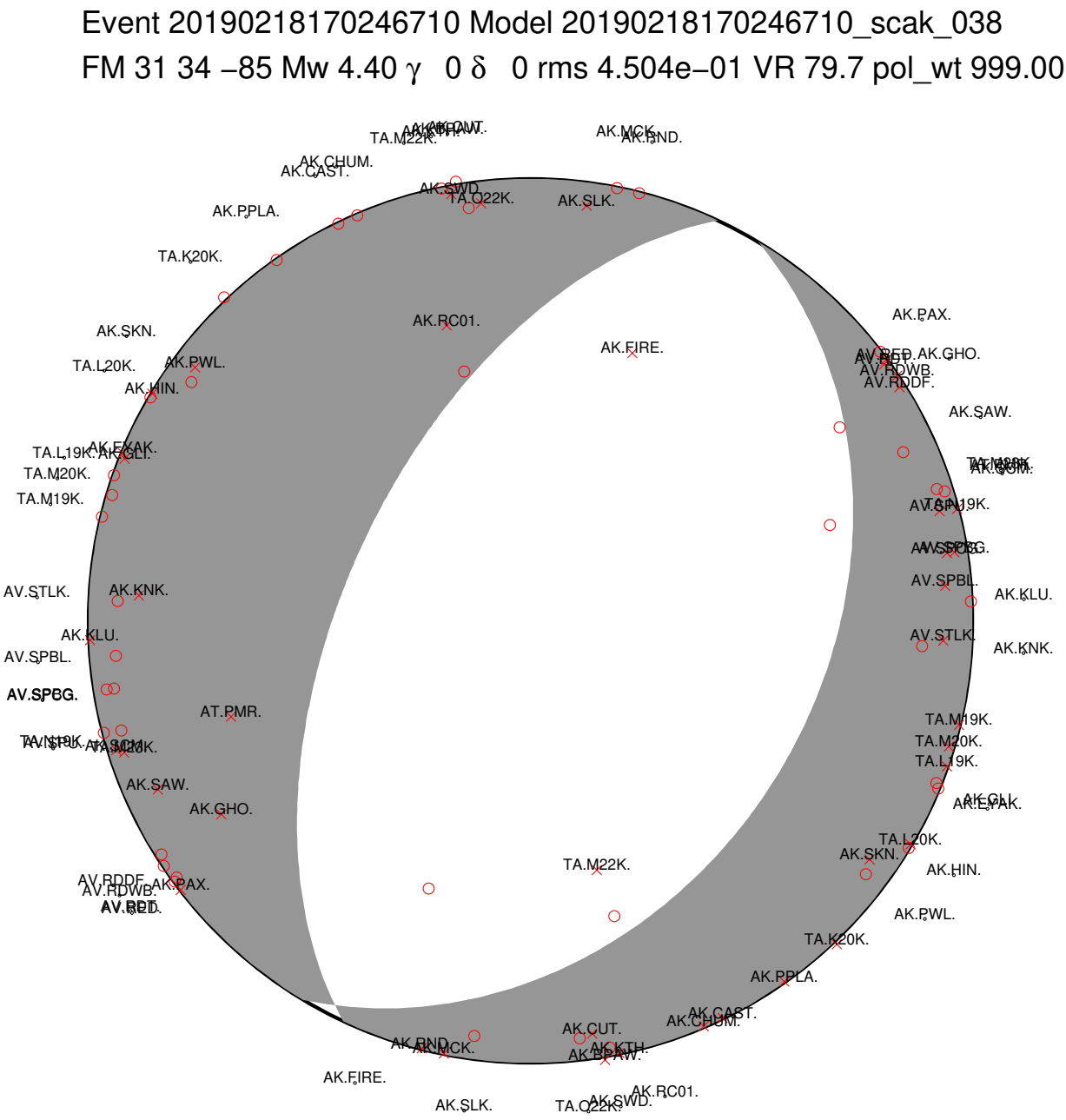

Figure M19: Same as Figure M4 except this is a solution for the 2018-11-30 M_w 7.1 Anchorage earthquakeaftershock, has 1 second allowable time shifts, and only includes permanent stations. Figure M18 displays the waveform fits for this event.